Highlights

- ✓ Ru – doped $LiCuFe_2O_4$ NPs revealed enhanced soft magnetic nature.
- ✓ Electrical properties under humidity suggest that this material can be used as capacitive as well as resistive humidity sensors.
- ✓ Simple route has been used to synthesize Ru – doped $LiCuFe_2O_4$ NPs.

Graphical Abstract

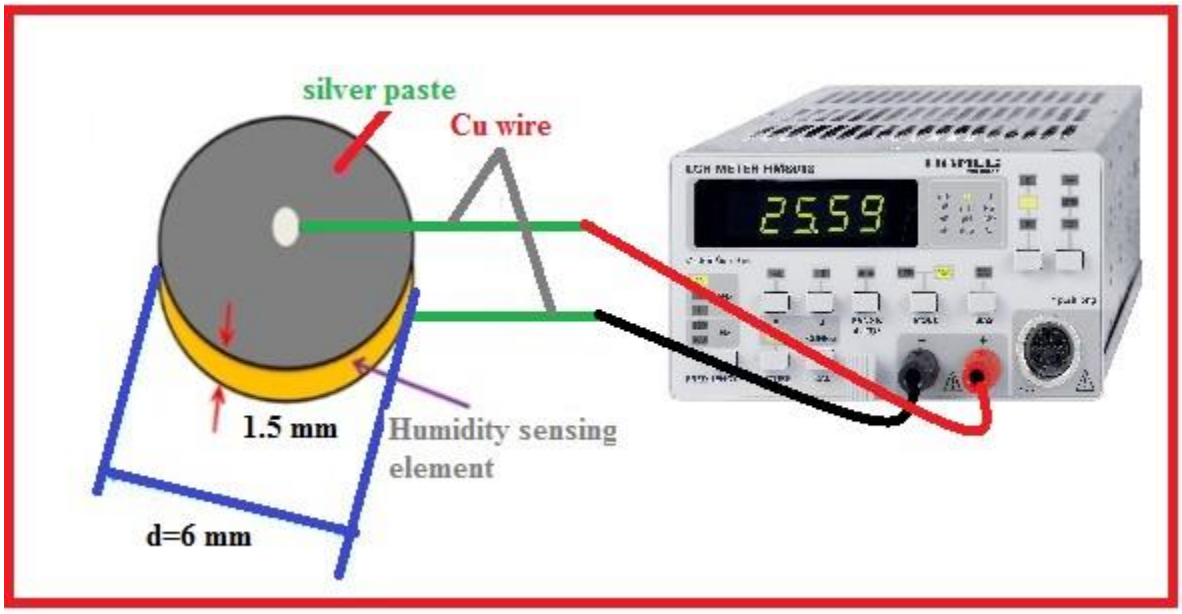

Fabrication and characterization of Ru-doped $LiCuFe_2O_4$ nanoparticles and their capacitive and resistive humidity sensor applications

V. Manikandan[a], Florin Tudorache[b], Iulian Petrila[c], R. S. Mane[d], V. Kuncser[e], Bogdan Vasile[f], David Morgan[g], S. Vigneselvan[h], Ali Mirzaei[i]*

[a]*Department of Physics, Kongunadu Arts and Science college, Coimbatore-641 029, India.*

[b]*Research Centre on Advanced Materials and Technologies, Interdisciplinary Research Department – Field Science, Alexandru Ioan Cuza University of Iasi, Bd. Carol I Nr. 11, Iasi 700506, Romania.*

[c]*Faculty of Automatic Control and Computer Engineering, Gheorghe Asachi Technical University of Iasi, Str. Dimitrie Mangeron, Nr. 27, Iasi 700050, Romania.*

[d]*Center for Nanomaterial & Energy Devices, Swami Ramanand Teerth Marathwada University, Dnyanteerth, Vishnupuri, Nanded-431606, India.*

[e]*National Institute of Materials Physics, Laboratory of Magnetism and Superconductivity, 405A Atomistilor Str., RO-77125 Magurele, Romania.*

[f]*University Politehnica of Bucharest, Gh. Polizu Street no.1-7, 011061 Bucharest, Romania.*

[g]*School of Chemistry, Cardiff University, Cardiff CF10 3AT, U.K.*

[h]*Department of Physics, Government College of Technology, Coibatore-641013 India.*

[i]*Department of Materials Science and Engineering, Shiraz University of Technology, Shiraz, Iran.*

(Corresponding author email address: manikandan570@gmail.com, (Dr.V. Manikandan)

Abstract

Polycrystalline ruthenium-doped lithium-copper-ferrite ($Ru - LiCuFe_2O_4$) nanoparticles (NPs) are synthesized using a simple and cost-effective chemical co-precipitation method and annealed at different temperatures for increasing the crystallinity. The transmission and scanning electron microscopy images have confirmed the presence of soft agglomerations and cuboids for the samples annealed at 1100°C. X-ray photoelectron results along with Raman spectra have collectively demonstrated the presence of Ru in the structure of $Ru - LiCuFe_2O_4$ NPs. The dielectric properties of as-synthesized $Ru - LiCuFe_2O_4$ NPs are investigated using LCR meter where the smaller NPs demonstrates a higher dielectric constant. Also, the results of magnetic measurements of annealed $Ru - LiCuFe_2O_4$ NPs have corroborated a soft magnetic nature due to the pinning sites that endow lower coercivity, remanence and saturation magnetization than that of the pristine one. The variation of permittivity and electrical resistivity with respect to frequency under humidity conditions suggested that this material has a potential to use as capacitive and resistive humidity sensor. The results of this study open the doors for utilization of metal-doped magnetic ferrites for humidity sensing applications.

Keywords: Magnetic properties; Electrical behavior; Humidity sensor; Particle size.

1. Introduction

Lithium-copper ferrites ($LiCuFe_2O_4$) have received considerable attention due to their unique electrical, dielectric and ferromagnetic properties which, basically, are dependent on the substitution of ions, preparation methods and annealing temperatures [1, 2]. Structural and morphological properties of $LiCuFe_2O_4$ can be tuned for improving the permeability and density [3] which are essential to realize data storage devices, gas and humidity sensors, microwave devices and cancer cell treatment etc. [4-6]. Furthermore, elemental substitutions can greatly influence the performance of ferrites on enhancing the electromagnetic performance. In this regards, $LiCuFe_2O_4$ as a well-known ferrite has very interesting properties [7-9]. It is found that the substitution of divalent metallic ions or rare earth ions significantly alters the magnetic properties [10-11]. The rare earth elements were doped in Mn, Mg-Zn, Ni-Zn and Mn-Zn ferrites to induce the soft magnetism [12-14] which eventually demonstrated special and desired physical properties. Among different metals, ruthenium (Ru) has been enormously used as a dopant to improve the magnetic performance. For example, Hoque *et al.* reported the enhanced magnetic properties of lithium-doped copper ferrite nanoparticles (NPs) as a hard magnetic material with higher coercivity and retentivity than that of undoped one [1]. Wenwei *et al.* reported the magnetic properties of copper-manganese lithium ferrite with highest specific saturation magnetization and retentivity values close to zero, suggesting a soft magnetic behavior [15]. Lithium-copper ferrite, reported by us previously, also revealed an inferior soft magnetic nature [9]. Raveau *et. al* reported that Ru doping can effectively induce the ferromagnetism. Arash *et al.* has reported manganese-doped zinc ferrite as dynamic adsorbents [16, 17]. Comparing to other elements like samarium, terbium, gadolinium etc., Ru has a strong stabilized ferromagnetic

nature because of its 4*d* metal character. Therefore, it is expected that in Ru - doped $LiCuFe_2O_4$ NPs, soft magnetic properties along with high magnetization can be easily achieved.

In this work, we unveil a facile wet chemical synthesis, characterization and a highly soft magnetic nature of Ru – doped $LiCuFe_2O_4$ NPs. The effects of doping and annealing temperature on the structure, morphology, dielectric and magnetic properties are explored. Generally, the ferrite material surfaces exhibit a myriads of open pores, making them as proof of concept research for humidity sensor device assembly [18]. Accordingly, Ru – doped $LiCuFe_2O_4$ samples are used to fabricate humidity sensor. The main use of humidity sensor is to monitor the relative humidity of environment [19]. Therefore, we also attempted to explore our material as humidity sensor

2. Experimental procedure

2.1 Synthesis of Ru - doped $LiCuFe_2O_4$NPs

Polycrystalline $Ru_xCu_{0.5-x}Li_{0.5}Fe_2O_4$ samples where x=0.1 was synthesized by a simple chemical co-precipitation method using phase pure $RuCl_3.2H_2O$,$CuCl_2.6H_2O$,$FeCl_3.9H_2O$ and LiCl as starting chemicals. According to stoichiometry, the starting materials were dissolved in 100 mL distilled water while continuous stirring till the solution turned to be light green in color. Subsequently, 100 mL of sodium chloride solution was slowly poured which caused to change the color of the solution to brown. The final solution was kept at 60 ℃ for 2h to complete the formation Ru – doped $LiCuFe_2O_4$ NPs, which were then washed thoroughly with de-ionized water to remove chloride content, if there could any, dried in hot-air oven overnight. As dried powders were transformed into a mortar agate for grinding process which was operated for 1 h

to produce a fine NPs with narrow size distribution. Finally, the NPs were annealed at muffle furnace for 5h to eliminate an organic residue. For electrical characterization, the samples were uniaxially pressed into disks of 6 mm diameter and of 1-1.5 mm thickness using a hydraulic pressure meter gauge.

2.2 Characterization details

The crystallinity and phase formation of the $\mathrm{Ru-doped\ LiCuFe_2O_4}$ NPs were examined by using X-ray diffractometer (XRD) with Rigaku Ultima III. The morphology was captured through JEOL 5600 SEM scanning electron microscopy (SEM) images. Transmission electron microscopy and selected area diffraction measurements were performed on Tecnai G2 F30S-TWIN to study the lattice spacing and crystallinity. Chemical compositions were studied using EPSRC X-ray photoelectron (XPS) spectroscopy. Raman spectroscopy was operated to confirm the formation of $\mathrm{Ru-doped\ LiCuFe_2O_4}$ NPs. The disk-shaped samples were polished and painted with silver contact electrodes on both sides. The dielectric measurements of the pressed samples were studied using LCR meter (Wayner Kerr 6500P). Magnetic measurements were conducted on vibrational sample magnetometer (VSM), Microsense Inc. USA (EZ9 model), equipped with a field of 2.2T. Humidity sensor analysis was done with help of LCR meter.

3. Results and Discussion

3.1 Structural analysis

Fig.1 presents the XRD patterns of $\mathrm{Ru-doped\ LiCuFe_2O_4}$NPs annealed in three different temperatures *viz.* for 5 h where the reflections at (220), (311), (400), (422), (511) and (440) reflection planes of

$LiCuFe_2O_4$ were obtained. All reflection peaks were indexed in

accordance with cubic phase of the $LiCuFe_2O_4$. From the XRD patterns, secondary phases were evolved in all samples. In ferrites evolution, formation of secondary phases one of the common practices can be assigned to the presence of iron vacancies in the sub-lattices which decreases with annealing temperatures [20]. With annealing temperatures, the peaks were broadening, implying an increase of the crystallinity. The average particle size was 5-41 nm.

3.2 Microstructural analysis

Fig. 2(a-b) depicts the SEM images of the $Ru-doped\ LiCuFe_2O_4$NPs annealed at 1100 ℃ at two different magnifications. The SEM images of the $Ru-doped\ LiCuFe_2O_4$ was composed ofcorroborated cuboids and nanorods. Also, the formation of soft agglomerated NPs was confirmed. Such kind of features would ensure high dielectric properties and moderate humidity sensing. Fig 2(c-d) highlights the TEM image of $Ru-doped\ LiCuFe_2O_4$NPs annealed at 1100 ℃ which was desirable annealed temperature for ferrite NPs preparation. Fig 2c shows the inhomogeneous particle formation with soft agglomeration, where the NPs with cuboids in shape were evidenced. Fig 2d describes the selected area electron diffraction (SAED) pattern of the $Ru-doped\ LiCuFe_2O_4$ NPs. Slightly less concentric rings and bright spots were seen, suggesting the formation of well-crystalline microstructure at elevated annealing temperatures [21].

3.3 Binding energy analysis

Fig. 3(a-f) describes the high resolution XPS spectra of $Ru-doped\ LiCuFe_2O_4$NPs annealed at 1100℃ scanned for knowing the elements and their binding energies. The carbon signal

located at 284.63 eV was due to the presence of air carbon species (Fig 3a). Fig. 3b depicts O 1s core-level region with two peaks; the peak around 529.67 eV was accredited to

lattice oxygen and the one located at 531.70 eV was attributed to the surface hydroxyl group [22]. Fig. 3c displays strong spectrum of Fe 2p around 710.70 eV for Fe $2p_{3/2}$ and 724.14 eV for Fe $2p_{1/2}$ [23,24]. Fig. 3d supplies three peaks of Cu around 933.41 eV for Cu $2p_{3/2}$ and 941.69 eV for Cu^{2+} satellite [25,26]. The third peak at 953.17 eV was from Cu $2p_{1/2}$. Fig. 3e displays Li 1s core level at 55.30 eV [25]. Finally, Fig. 3f reveals the Ru 3p core-level region with a peak located at 497.05 eV, suggesting effective doping of Ru in $LiCuFe_2O_4$ as $Ru-doped\ LiCuFe_2O_4$ [28].

3.4 Raman spectroscopy analysis

To confirm the formation of the $Ru-doped\ LiCuFe_2O_4$ NPs, Raman spectroscopy measurement was carried out at room-temperature and the obtained results are elucidated in Fig **4.** Raman spectra of 900 to 1100 ˚C temperature annealed samples were almost similar and bands were relatively broad. The synthesized ferrite NPs belonged to the cubic space group with first-order Raman active modes ($E_g+T_{2g}+2A_g$). Usually, ~ 785 cm^{-1} mode demonstrates the motion of oxygen in tetrahedral sub-lattice that of lower modes demonstrate the vibrational mode of octahedral sublattice [29]. In Fig 1, four Raman modes are obtained at 280, 777, 1534 and 1724 cm^{-1} which were assigned to E_g, T_{2g} and $2A_g$, respectively. Raman intensity was reduced on increasing of the annealing temperature from 1000 to 1100 ºC. This behavior was due to the formation of ion vacancies and lattice defects at octahedral sites. Additionally, the modes at 1534 and 1724 were noted on account of the cation redistribution at tetrahedral sites, suggesting an effective Ru doping [30].

3.5 Dielectric properties

The variation of dielectric constant with respect to frequency at room-temperature for the $Ru-doped\ LiCuFe_2O_4$ disc shaped pellets annealed at different temperatures is shown in Fig 5a. In all samples, dielectric constant increased and then decreased with respect to frequency. At high frequency, dielectric constant decreased which is one of the common behaviors in ferrite structures [31, 32]. The variation in dielectric constant with respect to frequency demonstrated the dispersion, in agreement with Koop's theory, which was characterized through a space charge polarization method. According to Koop's theory, from conductivity point of view, as- obtained ferrites were composed of two layers namely conducting and poor conducting [33]. The well-conducting grains belonged to high frequency region and a poor conducting grains were of low frequency region [34]. High dielectric constant was achieved at low frequency because the number electrons could be piled or displaced at poor conducting grains which led to maximize the space charge of polarization. Likewise, low dielectric constant was achieved at high frequency due to interruption of electron displacement, leading to decrease of the space charge polarization. However, electron displacement between the well and poor conducting grains might be interrupted on localizing the charge accumulation at the interface. Also, the electron displacement between Fe^{2+} and Fe^{3+} ions cannot follow alternate field, resulting a low space-charge polarization [35]. Dielectric constant depends on the particle size, where small-sized particles offer large surface grain boundaries and reveal a high dielectric constant. On the other hand, large sized particles demonstrate lower surface grain boundaries, revealing a low dielectric constant. Fig. 5b shows the variation of dielectric loss with respect to frequency. At high frequency, as the jumping frequency of electric charge carriers cannot follow the alternate field, dielectric loss decreases. The variation of dielectric loss with respect to frequency, initially, showed relaxation peak which due to relaxation in dipole was shifted to higher frequency side.

Such dipoles occur due to electronic, space charge, molecular polarization etc., relaxing at different frequencies [36].

3.6Magnetic properties

Fig. 6(a-c) describes the hysteresis loop of $Ru-doped\ LiCuFe_2O_4$NPs annealed at different temperatures. The measurement was carried out at room-temperature. Under the influence of applied field, the $Ru-doped\ LiCuFe_2O_4$NPs confirmed a clear soft magnetic hysteresis behavior. Due to the elements occupied sites, the synthesized NPs demonstrated ferrimagnetic nature [37]. Based on the literature survey, the elements like lithium, copper and ruthenium occupy in octahedral sites whereas, the iron occupies in tetrahedral sites. According to ferrimagnetic nature of ferrites, the magnetic moments in octahedral and tetrahedral sites were aligned antiparallel. Likewise, magnetic moment of rare earth elements originated from 4d electrons is characterized by a low magnetic ordering temperature (below 60 K) and exhibits disorder magnetic dipolar orientation. Therefore, ruthenium is considered to be non-magnetic [37]. From Fig 6, the magnetization increased with annealing temperature as the particle size increases with annealing temperature, resulting in development of well-crystallized microstructure. Correspondingly, the number of grain boundaries increased and then the amounts of surface and interfaces also increased, supplying more pinning sites for domain wall motions [38,39]. Also, the domain walls might coincide with the grain boundaries [40], suggesting $Ru-doped\ LiCuFe_2O_4$NPs were in soft magnetic character. Refereeing to our previous report on $Li-CuFe_2O_4$ NPs, the contribution of domain wall displacement was high on magnetization process, implying an increase of both high magnetization and soft magnetic behaviors on doping process [9,37]. Likewise, in this study, the saturation magnetization values increased due to Ru

doping, suggesting the growth of magnetization process. The obtained high magnetization in Ru - doped $LiCuFe_2O_4$ NPs was a result antiparallel sublattice magnetization of Fe^{3+} balancing [49]. Hence, the effect of ruthenium substitution was entirely different from other non-magnetic elements in octahedral sites. The $Ru-doped\ LiCuFe_2O_4$NPs revealed superior paramagnetic behavior at 900 and 1000℃ where, coercivity and remnance magnetization values were zero. At 1100℃, $Ru-doped\ LiCuFe_2O_4$ NPs showed smaller values of coercively and remanence magnetization. It has been reported that high coercivity, saturation magnetization and low remanence are essential for data storage device applications [41].

3.7 Humidity sensing properties

For humidity sensing applications, the electrical permittivity and electrical resistance measurements were performed in the range of 20 Hz – 20 MHz at room-temperature, in an enclosure box with a known relative humidity (RH) in 0-97% RH range. From the investigation, the relative permittivity and electrical resistivity of annealed samples showed frequency dependence. From Fig 7and 8, the electrical resistivity and relative permittivity were respectively obtained as a function of frequency which was in accordance with Koop's phenomenological theory. The obtained dielectric dispersion was explained on the basis of Maxwell-Wagner-type of interfacial or space-charge polarization [42, 43]. The relative permittivity demonstrated a higher relative change in the range from 0 to 97%RH than the relative change of electrical resistivity, which in fact was more informative. The relative permittivity values were high even at low frequency range (Fig. 7). In this range, maximum conductivity across the grain boundaries led to high permittivity. Also, the high sensitivity of electrical resistivity to RH change was appeared in low frequency. The relative permittivity decreased at high frequency owing to the $Fe^{3+} \leftrightarrow Fe^{2+}$ electronic displacement and because of predominance species like oxygen

vacancy, lattice defects and Fe^{2+} ions, it was free from the alternate field [44, 47]. The sample

annealed at 1100 ℃ showed a maximum relative permittivity as compared to 900 and 1000 ℃ samples, which was attributed to maximum space charge polarization. The relative permittivity is influenced by number of parameters like frequency, crystallinity, pore size and pore-size distribution [44]. Based on Figs. 7 and 8, increase in the relative permittivity and decrease in the electrical resistivity could be appreciated in the humidity sensor application. The Ru – doped $LiCuFe_2O_4$NPs exhibited increasing nature of the relative permittivity and decreasing nature of the electrical resistivity which could be due to Maxwell-Debye relaxation where, the open pores are filled with water vapors pores [45,47]. The variation of electrical resistivity and permittivity with respect to frequency under humidity suggested that this material was of potential candidate to be used as humidity sensor. As it can be seen in Fig. 7, under different humidity conditions, the permittivity response showed maximum variations for the Ru – doped $LiCuFe_2O_4$NPs annealed at 1000 C, demonstrating suitability for application in capacitive humidity sensors. The electrical resistance measurements suggested that the Ru – doped LiCu Fe_2O_4NPs annealed at 900 C revealed smaller particles and showed a maximum variation of electrical resistivity at different humidity levels (Fig. 8). Consequently, at lower frequencies, this material could act as active material for realization of resistive humidity sensors.

5. Conclusion

In brief, Ru – doped LiCuFe2O4 NPs were successfully synthesized by a facile chemical co-precipitation method followed by annealing treatment at various temperatures (900-1100°C). XRD results confirmed the formation of well-crystalline ferrites and the morphology studies by SEM and TEM microscopes demonstrated the presence of soft agglomerations of cuboids and nanorods. Also based on the XPS and Raman analyses, the presence of Ru was in the synthesized products was confirmed. According to magnetic studies, upon substitution of Ru, a soft magnetic

behavior was induced in all samples. Dielectric constant and dielectric loss of as-fabricated pellets of Ru − doped $LiCuFe_2O_4$ annealed at different temperatures were studied as a function of frequency, where in agreement with Koop's theory, they demonstrates the dispersion which can be characterized by space charge polarization. Finally, the study of the variations of dielectric constant and electrical resistance in the presence of various RH (0-97%), demonstrated the possibility of using of Ru − doped $LiCuFe_2O_4$ as a humidity sensor, in which, the resistance values decreased, while dielectric constants were increased. These results suggests the search for finding of more sensitive ferrite samples for practical applications such as humidity and gas sensors.

References

[1] D. K. S. S. ManjuraHoque M.SamirUllah , F.A.Khan , M.A.Hakim, Structural and magnetic properties of Li–Cu mixed spinel ferrites.Phys. B, 2011, **206**, 1799–1804.

[2] V. Manikandan, M. Singh, B. C. Yadav and J. C. Denardin, Fabrication of Lithium substituted Copper ferrite (Li-$CuFe_2O_4$) thin film as an efficient gas sensor at room temperature, J. Sci. Adv. Mater. Devices, , DOI:10.1016/j.jsamd.2018.03.008.

[3] Y. Zhou, W. Chen, Y. Shen, X. Wu, W. Wu and J. Wu, Lattice strains and magnetic properties evolution of copper-magnesium ferrite with lithium substitution,J. Magn. Magn. Mater., 2015, **396**, 198–203.

[4] M. Singh, B. C. Yadav, A. Ranjan, R. K. Sonker and M. Kaur, Detection of liquefied petroleum gas below lowest explosion limit (LEL) using nanostructured hexagonal strontium ferrite thin film,Sensors Actuators, B Chem., 2017, **249**, 96–104.

[5] V. Manikandan, S. Sikarwar, B. C. Yadav and R. S. Mane, Fabrication of Tin substituted Nickel Ferrite (Sn-$NiFe_2O_4$) Thin film and its application as humidity sensorSensors Actuators A. Phys., , DOI:10.1016/j.sna.2018.01.059.

[6] E. Fantechi, C. Innocenti, M. Zanardelli, M. Fittipaldi, E. Falvo, M. Carbo, V. Shullani, L. Di Cesare Mannelli, C. Ghelardini, A. M. Ferretti, A. Ponti, C. Sangregorio and P. Ceci, A smart platform for hyperthermia application in cancer treatment: Cobalt-doped ferrite nanoparticles mineralized in human ferritin cages,ACS Nano, 2014, **8**, 4705–4719.

[7] P. A. Shaikh, R. C. Kambale, A. V. Rao and Y. D. Kolekar, Studies on structural and electrical properties of $Co_{1-x}Ni_xFe_{1.9}Mn_{0.1}O_4$ferrite,J. Alloys Compd., 2009, **482**, 276–282.

[8] Z. K. Heiba, M. B. Mohamed, A. M. Wahba and L. Arda,Magnetic and Structural Properties of Nanocrystalline Cobalt-Substituted Magnesium–Manganese Ferrite,J. Supercond. Nov. Magn., 2015, **28**, 2517–2524.

[9] V. Manikandan, A. Vanitha, E. R. Kumar and S. Kavita,Influence of sintering temperature on structural, dielectric and magnetic properties of Li substituted $CuFe_2O_4$ nanoparticles,J. Magn. Magn. Mater., 2017, **426**, 11–17.

[10] X. Cao, K. Sun, C. Sun and L. Leng, The study on microstructure and microwave- absorbing properties of lithium zinc ferrites doped with magnesium and copper,J. Magn. Magn. Mater., 2009, **321**, 2896–2901.

[11] S. R. Naik and A. V. Salker, Change in the magnetostructural properties of rare earth doped cobalt ferrites relative to the magnetic anisotropy,J. Mater. Chem., 2012, **22**, 2740– 2750.

[12] Q. Xing, Z. Peng, C. Wang, Z. Fu and X. Fu, Doping effect of Y^3ions on the microstructural and electromagnetic properties of MnZn ferrites,Phys. B Condens. Matter, 2012, **407**, 388–392.

[13] N. Lwin, M. N. Ahmad Fauzi, S. Sreekantan and R. Othman,Physical and electromagnetic properties of nanosized Gd substituted Mg-Mn ferrites by solution combustion method,Phys. B Condens. Matter, 2015, **461**, 134–139.

[14] S. E. Jacobo, S. Duhalde and H. R. Bertorello, Rare earth influence on the structural and magnetic properties of NiZn ferrites,J. Magn. Magn. Mater., 2004, **272**–**276**, 2253–2254.

[15] W. Chen, Y. Zhou, J. Lu, X. Huang, W. Wu, C. Lin and Q. Wang, Effects of

Li^{+}substitution on the structural and magnetic properties of $Co_{0.5}Mn_{0.5}Fe_2O_4$ particlesCeram. Int., 2016, **42**, 1114–1121.

[16] Arash Asfaram, Mehrorang Ghaedi, Kheibar Dashtian, and Gholam Reza Ghezelbash, Preparation and Characterization of $Mn_{0.4}Zn_{0.6}Fe_2O_4$ Nanoparticles Supported on Dead Cells of Yarrowia lipolytica as a Novel and Efficient Adsorbent/Biosorbent Composite for the Removal of Azo Food Dyes: Central Composite Design Optimization Study, ACS Sustainable Chem. Eng. 2018, 6, 4549−4563.

[17] Arash Asfaram, Mehrorang Ghaedi, Hassan Abidi, Hamedreza Javadian, Mohammad Zoladl, Fardin Sadeghfar, Synthesis of Fe_3O_4@CuS@Ni_2P-CNTs magnetic nanocomposite for sonochemical- assisted pre-concentration of trace Allura Red from aqueous samples prior to HPLC-UV detection: CCD-RSM design, Ultrasonics Sonochemistry 44, 2018, 240-250.

[18] B. C. Yadav, S. Sikarwar, A. Bhaduri and P. Kumar, Characterization and Development of Opto-Electronic Humidity Sensor using Copper Oxide Thin Film,2015, **2**, 105–109.

[19] S. Sikarwar and B. C. Yadav, Opto-electronic humidity sensor: A review, Sensors Actuators, A Phys., 2015, **233**, 54–70.

[20]. D. Maiti, U. Manju, S. Velaga and P. S. Devi, Phase Evolution and Growth of Iron Oxide Nanoparticles: Effect of Hydrazine Addition During Sonication,Cryst. Growth Des., 2013, **13**, 3637–3644.

[21] S. E. Shirsath, M. L. Mane, Y. Yasukawa, X. Liu and A. Morisako, Self-ignited high temperature synthesis and enhanced super-exchange interactions of Ho(3+)–Mn(2+) –Fe(3+)–O(2−) ferromagnetic nanoparticles, Phys. Chem. Chem. Phys., 2014, **16**,

2347–2357.

[22] E. Poonia, P. K. Mishra, V. Kiran, J. Sangwan, R. Kumar, P. K. Rai and V. K. Tomer,Aero-gel assisted synthesis of anatase TiO_2nanoparticles for humidity sensing application,Dalt. Trans., , DOI:10.1039/c8dt00106e.

[23] A. Mirzaei, K. Janghorban, B. Hashemi, M. Bonyani, S. G. Leonardi and G. Neri, Highly stable and selective ethanol sensor based on α-Fe_2O_3 nanoparticles prepared by Pechini sol–gel method,Ceram. Int., 2016, **42**, 6136–6144.

[24] D. D. Hawn and B. M. DeKoven, Deconvolution as a correction for photoelectron inelastic energy losses in the core level XPS spectra of iron oxides,Surf. Interface Anal., 1987, **10**, 63–74.

[25] C. Calderón, P. Bartolo-Pérez, O. Rodríguez and G. Gordillo, Phase identification and XPS studies of Cu(In,Ga)Se_2thin films,Microelectronics J., 2008, **39**, 1324–1326.

[26] M. T. Marques, A. M. Ferraria, J. B. Correia, A. M. B. do Rego and R. Vilar, XRD, XPS and SEM characterisation of Cu-NbC nanocomposite produced by mechanical alloying,Mater. Chem. Phys., 2008, **109**, 174–180.

[27] A. Lahiri, N. Borisenko, A. Borodin, M. Olschewski and F. Endres,Characterisation of the solid electrolyte interface during lithiation/delithiation of germanium in an ionic liquid,Phys. Chem. Chem. Phys., 2016, **18**, 5630–5637.

[28] X. Meng, H. Li, J. Chen, L. Mei, K. Wang and X. Li, Mössbauer study of cobaltferrite nanocrystals substituted with rare-earth Y^{3+} ions, J. Magn. Magn. Mater. 321(2009) 1155–1158.

[29] Xiruo Zhao, Wei Wang, Yajun Zhang, Sizhu Wu, Feng Li, J. Ping Liu, Synthesis and characterization of Gadolinium doped Cobalt ferrite nanoparticleswith enhanced adsorption capability for Congo Red, Chem.Eng.Jour. 250, (2014), 164-174.

[30] Y. Park, B. Lee, C. Kim, Y. Oh, S. Nam and B. Park, The effects of ruthenium-oxidation states on Ru dissolution in PtRu thin-film electrodes,J. Mater. Res., 2009, **24**, 2762–2766.

[31] A. D. S. Æ. V. L. Mathe, M. A. Gabal and Y. M. Al Angari, Effect of diamagnetic substitution on the structural, magnetic and electrical properties of $NiFe_2O_4$, Mater. Chem. Phys., 2009, **115**, 578–584.

[32] A. D. Sheikh and V. L. Mathe, Anomalous electrical properties of nanocrystalline Ni-Zn ferrite, J. Mater. Sci., 2008, **43**, 2018–2025.

[33] V. Manikandan, A. Vanitha, E. Ranjith Kumar and J. Chandrasekaran,ffect of sintering temperature on Structural and Dielectric properties of Sn substituted $CuFe_2O_4$ Nanoparticles, J. Magn. Magn. Mater., 2017, **423**, 250–255.

[34] T. J. Shinde, A. B. Gadkari and P. N. Vasambekar, Effect of Nd^{3+}substitution on structural and electrical properties of nanocrystalline zinc ferrite,J. Magn. Magn. Mater., 2010, **322**, 2777–2781.

[35] S. S. Jadhav, S. E. Shirsath, B. G. Toksha, S. M. Patange, D. R. Shengule, K. M. Jadhav, T. Jahanbin, M. Hashim, K. Amin Mantori, C. Venkataraju, G. Sathishkumar and K. Sivakumar, Effect of nickel on the electrical properties of nanostructured MnZn ferrite,J. Alloys Compd., 2010, **322**, 203–206.

[36] S. S. Jadhav, S. E. Shirsath, B. G. Toksha, S. M. Patange, D. R. Shengule and K. M.

Jadhav, Structural and electric properties of zinc substituted $NiFe_2O_4$ nanoparticles prepared by co-precipitation method, Phys. B Condens. Matter, 2010, **405**, 2610–2614.

[37] M. F. Al-Hilli, S. Li and K. S. Kassim, Structural analysis, magnetic and electrical properties of samarium substituted lithiumnickel mixed ferrites, J. Magn. Magn. Mater., 2012, **324**, 873–879.

[38] M. Taheri, E. E. Carpenter, V. Cestone, M. M. Miller, M. P. Raphael, M. E. McHenry and V. G. Harris, Magnetism and structure of $Zn_xFe_{3-x}O_4$ films processed via spin-spray deposition, J. Appl. Phys., 2002, **91**, 7595–7597.

[39] C. Venkata Reddy, C. Byon, B. Narendra, D. Baskar, G. Srinivas, J. Shim and S. V. Prabhakar Vattikuti, Investigation of structural, thermal and magnetic properties of cadmium substituted cobalt ferrite nanoparticles,Superlattices Microstruct., 2015, **82**, 165–173.

[40] S. Ren, C. Lu, H. Shen and Y. Wang, In situ study of the evolution of domain structure in free-standing polycrystalline thin films under external stress,Phys. Rev. B - Condens. Matter Mater. Phys., 1997, **55**, 3485–3489.

[41] Z. A. Gilani, M. F. Warsi, M. N. Anjum, I. Shakir, S. Naseem, S. Riaz and M. A. Khan,Structural and electromagnetic behavior evaluation of Nd-doped lithium-cobalt nanocrystals for recording media applications,J. Alloys Compd., 2015, **639**, 268–273.

[42] R. B. Hilborn, Maxwell-Wagner polarization in sintered compacts of ferric oxide,J. Appl. Phys., 1965, **36**, 1553–1557.

[43] A. Jawad, A. S. Ahmed, S. S. Z. Ashraf, M. Chaman and A. Azam, Exploring the

dielectric behaviour of nano-structured Al^{3+} doped $BiFeO_3$ ceramics synthesized by auto ignition process,J. Alloys Compd., 2012, **530**, 63–70.

[44] A. M. Dumitrescu, G. Lisa, A. R. Iordan, F. Tudorache, I. Petrila, A. I. Borhan, M. N. Palamaru, C. Mihailescu, L. Leontie and C. Munteanu, Ni ferrite highly organized as humidity sensors,Mater. Chem. Phys., 2015, **156**, 170–179.

[45] F. Tudorache, I. Petrila, P. D. Popa and S. Tascu, Influence of thermal treatment on the structure, humidity sensitivity, electrical and magnetic properties of barium-tungsten ferrite, Compos. Part B Eng., 2013, **51**, 106–111.

[46] Z.V. Mocanu, M. Airimioaei, C.E. Ciomaga, L. Curecheriu, F. Tudorache, S. Tascu, A.R. Iordan, N.M. Palamaru, L. Mitoseriu, Investigation of the functional properties of $Mg_xNi_{1-x}Fe_2O_4$ ceramicsJ. Materials Science49 (2014) 3276-3286.

[47] I. Petrila, F. Tudorache, Humidity sensor applicative material based on copper-zinc-tungsten spinel ferrite, M. Letters**108** (2013) 129-133.

[48] Raveau, B.; Maignan, A.; Martin, C.; Hervieu, M.Ru doping of perovskite manganites: an effective route to ferromagnetism, metallicity, and CMR, J. Supercond. **2001**, 14, 217.

[49] Wang, J.; Scholl, A.; Ogale, S. B.; Viehland, D.; Schlom, D. G.; Scott, J. F.; Mathur, N. D. Technical comment abstracts,Science **2005**, 307, 1203

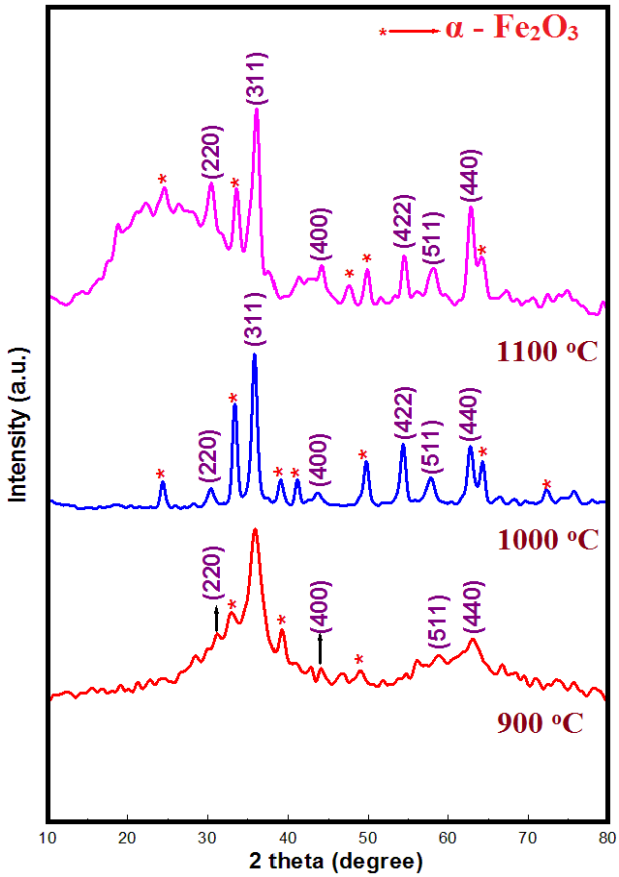

Fig. 1 XRD patterns of Ru – doped $LiCuFe_2O_4$ NPs at different annealing temperatures

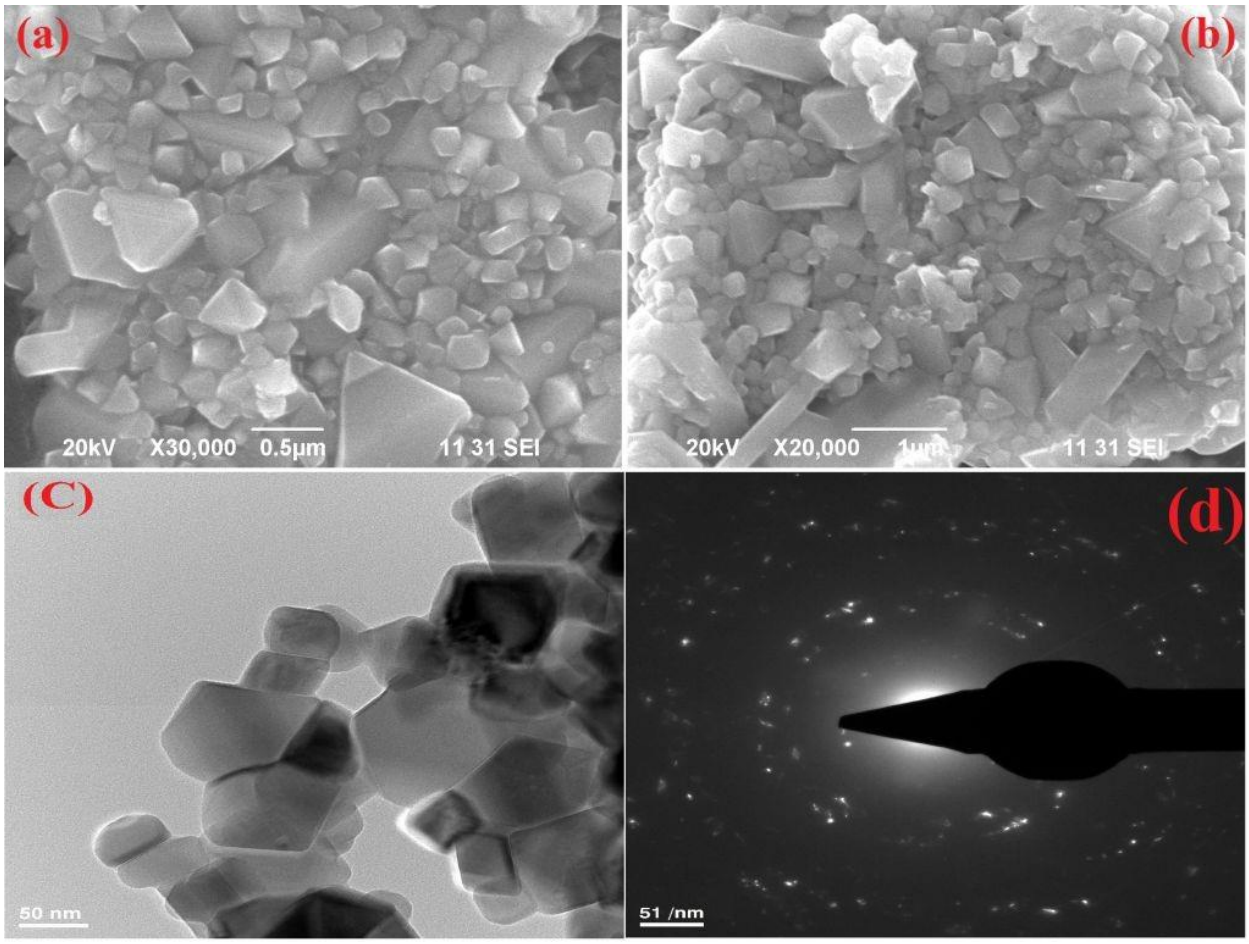

Fig. 2 (a-b) SEM, (c) TEM and (d) SAED pattern images of Ru − doped $LiCuFe_2O_4$ NPs annealed at 1100℃

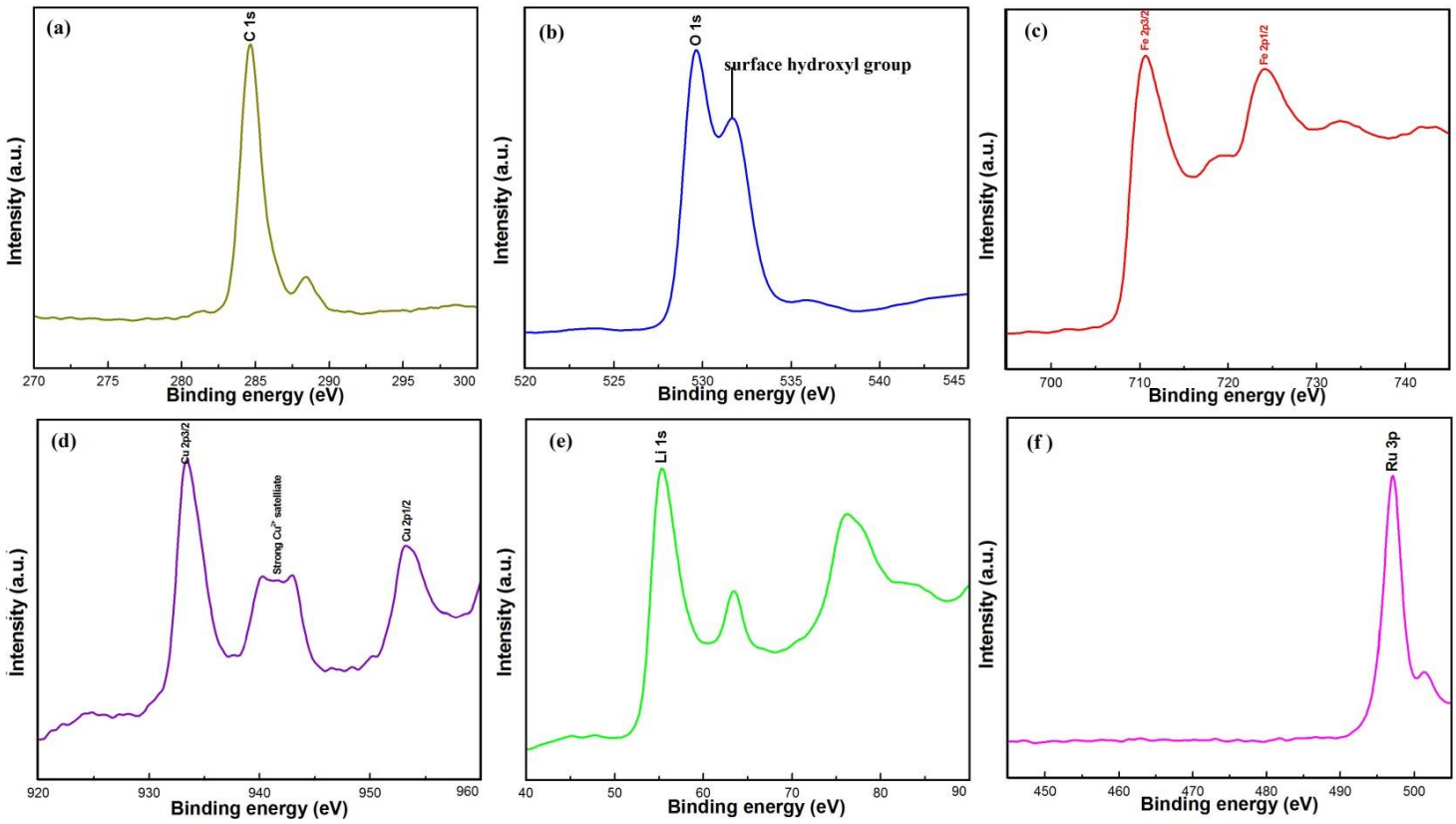

Fig. 3 XPS spectra of the Ru − doped $LiCuFe_2O_4$ NPs annealed at 1100℃

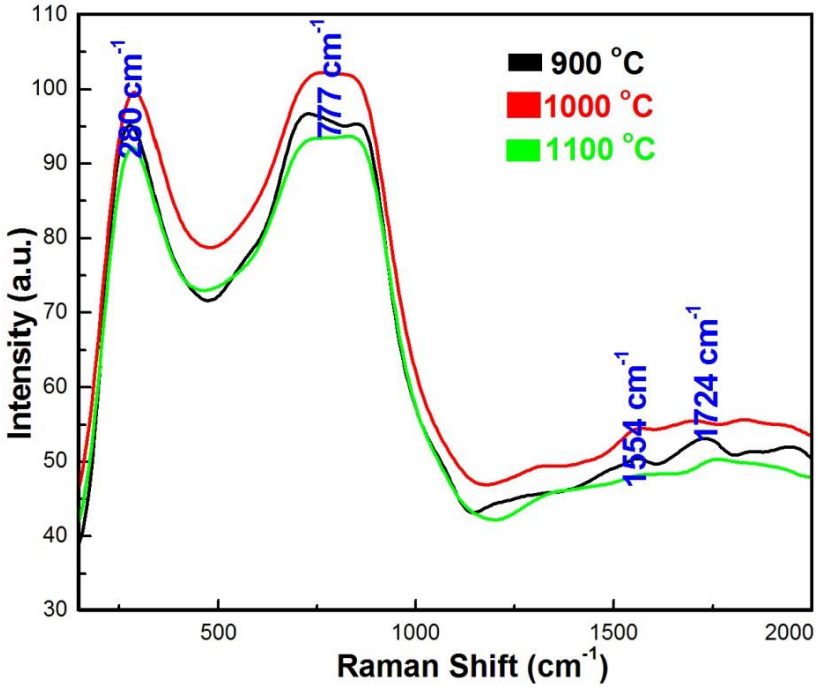

Fig. 4 Raman spectra of Ru − doped $LiCuFe_2O_4$ NPs for various annealing temperatures

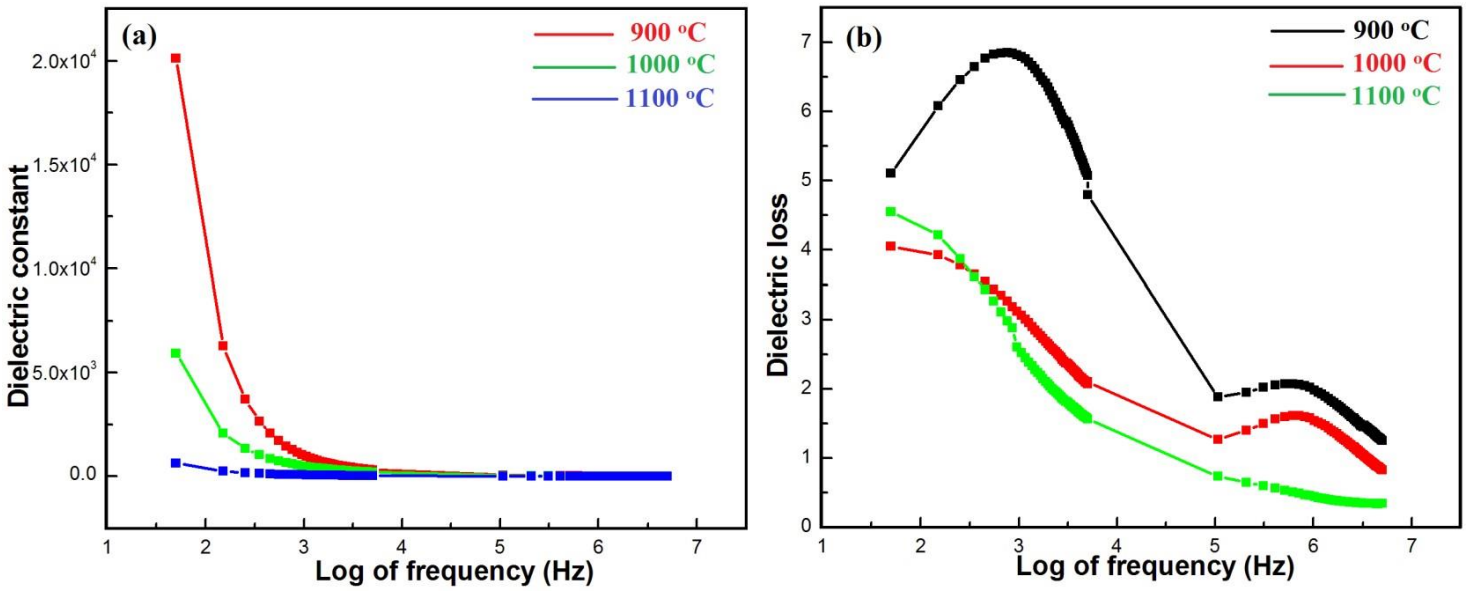

Fig. 5. (a) Dielectric constant, and (b) dielectric loss of Ru – doped $LiCuFe_2O_4$ NPs annealed at different temperatures.

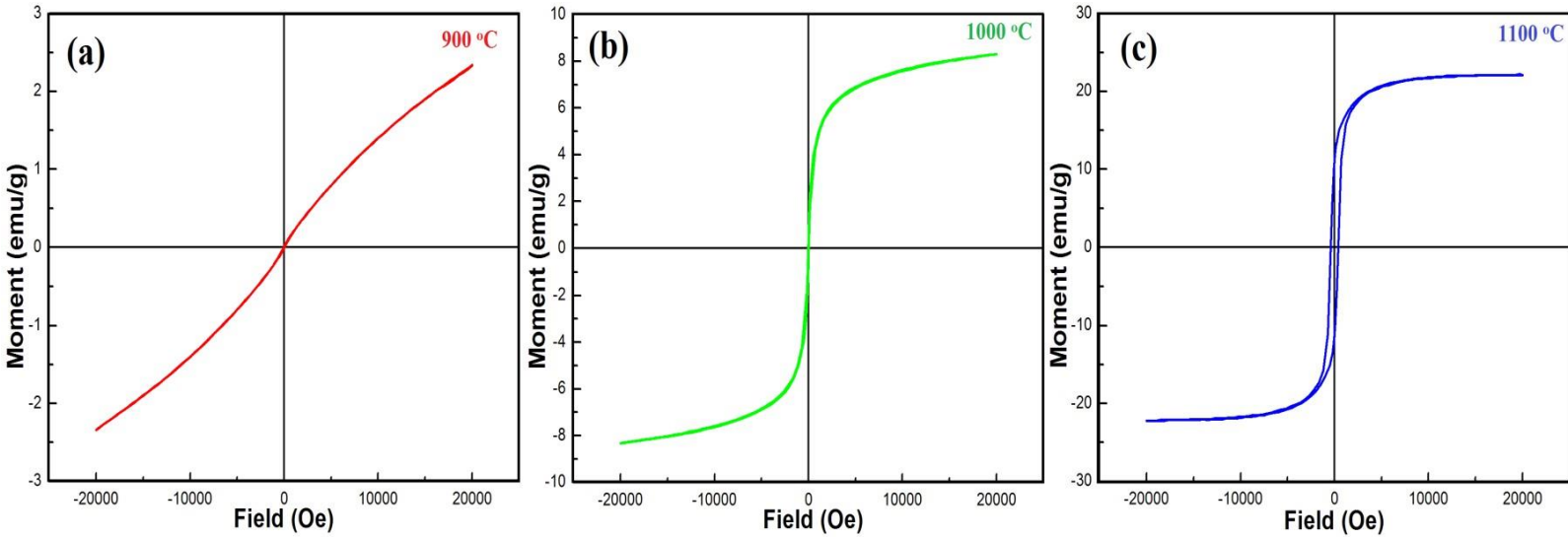

Fig. 6. Hysteresis loops of Ru – doped $LiCuFe_2O_4$ NPs annealed at various temperatures

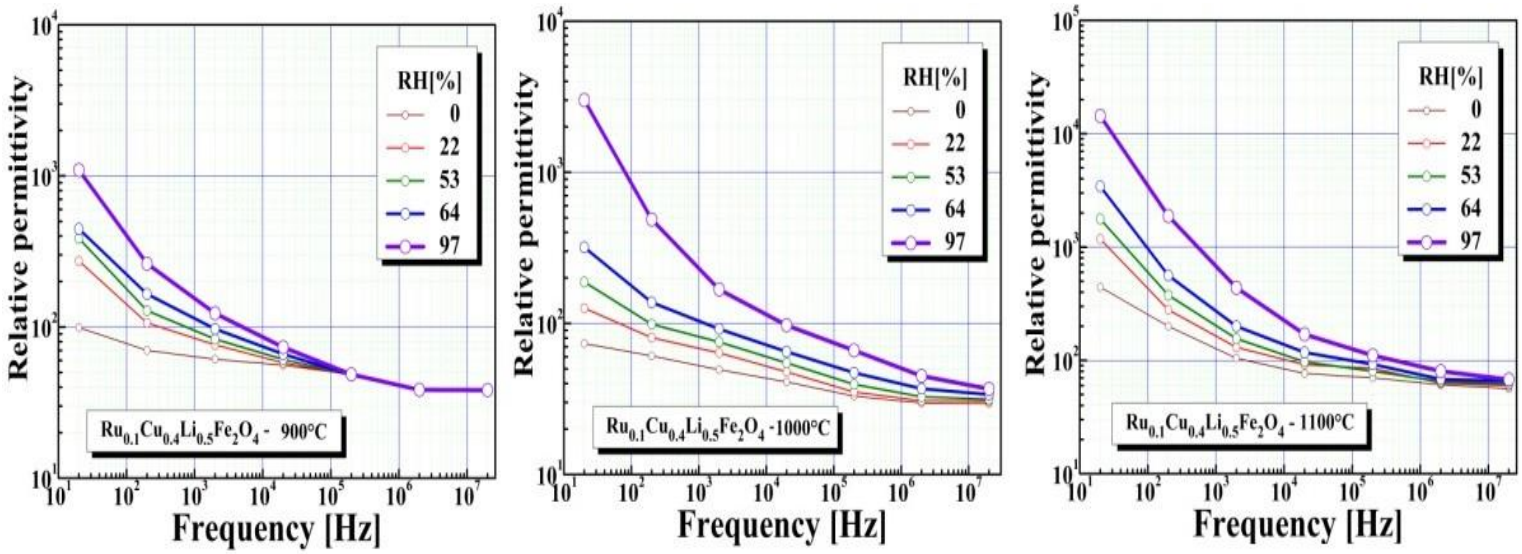

Fig. 7.Variation of relative electrical permittivity *vs*. frequency for different relative humidity levels.

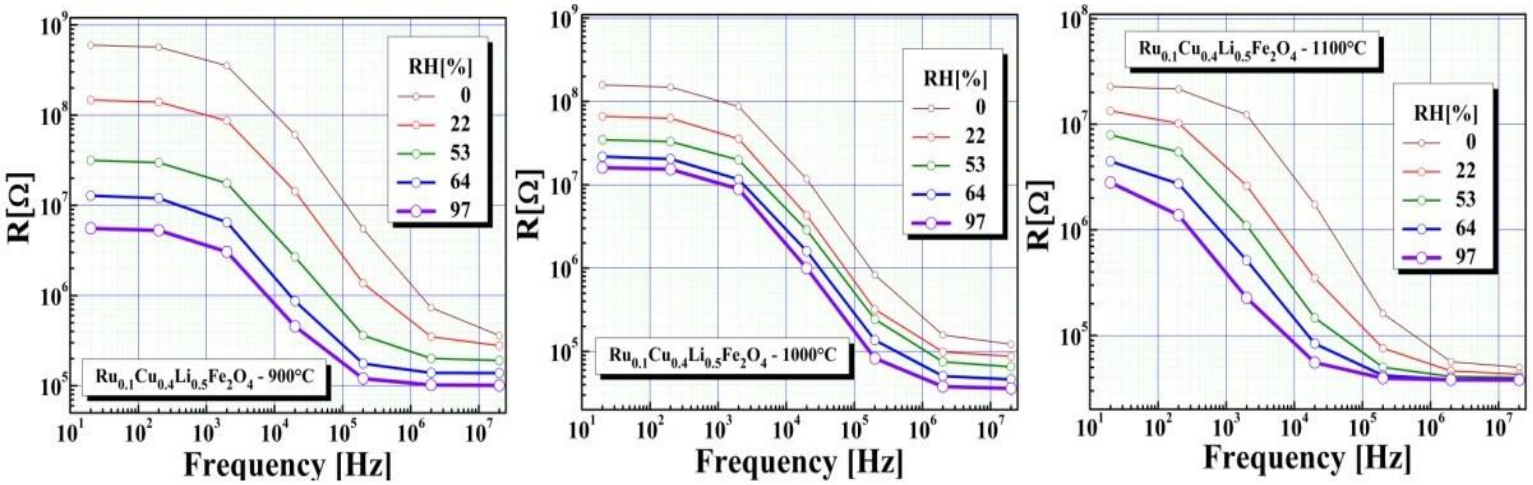

Fig. 8 Variation of relative electrical resistivity *vs*. frequency for different relative humidity levels

Table 1 shows the XRD, dielectric and Magnetic parameters of Ru − doped $LiCuFe_2O_4$ NPs

Parameters	$Ru - LiCuFe_2O_4$ $(Ru_{0.1}Cu_{0.4}Li_{0.5}Fe_2O_4)$		
Temperature (°C)	**900**	**1000**	**1100**
Particle size (nm)	5	27	41
Dielectric constant (ε)	617.39	261.22	37.96
Dielectric loss (D)	3.85	1.93	1.30
Coercivity (Oe)	-	-	388.71
Remanence (emu/g)	-	-	10.73
Saturation (emu/g)	-	7.91	21.08